

# Control Strategy for Five-Phase Dual-Stator Winding Induction Starter/Generator System

Haozhe Liu, Feifei Bu, *Member, IEEE*, Wenxin Huang, *Member, IEEE*, Lu Liu, Yuwen Hu, *Member, IEEE*, Michele Degano, *Member, IEEE*, and Chris Gerada, *Senior Member, IEEE*,

**Abstract**— This paper presents an integrated control strategy for a starter/generator (S/G) system based on five-phase dual-stator winding induction machine (FPDWIM). The FPDWIM has a cage-type rotor and two sets of stator windings. One is a five-phase control winding (CW) and the other is a five-phase power winding (PW). In the starting mode, the FPDWIM works as a motor. The CW provides both active power and reactive power to drive the engine. In the generating mode, the CW mainly handles reactive power while the PW outputs active power. To achieve the integration of the starting and generating controls, indirect CW-flux-oriented control (ICWFOC) is proposed to operate in both starting and generating modes. In starting mode, the CW current and flux are controlled to output a constant starting torque; while in generating mode, both CW and PW DC bus voltages are regulated. In this way, the principles and structures of the control strategies in both modes are compatible, resulting in a simpler implementation and improved performance. With the proposed control strategy, the system can complete the starting-generating operation with a smoother transition process. Simulation and experimental results are compared to validate the proposed control strategy.

**Index Terms**— Five-phase, induction machine, dual stator winding, starter/generator, ICWFOC, smooth transition control.

## NOMENCLATURE

$u$	Voltage.
$i$	Current.
$\psi$	Flux.
$T_e$	Electromagnetic torque.
$n_r, n_c$	Rotor speed, stator mmf speed.
$n_i, n_g$	Ignition speed, generating speed.
$\omega_c$	Stator angular frequency.

$\omega_s$	Slip angular frequency.
$\omega_{ci}$	Stator angular frequency at ignition speed.
$\omega_{cg}$	Stator angular frequency at generating speed.
$n_p$	Pole pairs.
$p$	Differential operator.
$p_c, q_c$	CW active and reactive power.
$R$	Resistance.
$L$	Inductance.
$l$	Leakage inductance.
$D$	Diode.
$C$	Capacitor.
$\theta_c$	Orientation angle.
<i>Subscript</i>	
$abcde$	Control winding phase $a, b, c, d, e$ .
$c, r, p$	CW, PW and rotor.
1, 2, 3, 4,	Step 1, 2, 3, 4.
$d, q$	$d$ -axis, $q$ -axis.
$\alpha, \beta$	$\alpha$ -axis, $\beta$ -axis.
DC	DC bus.
$l$	Load.

## I. INTRODUCTION

THE rapid development of the power systems in more/all electric aircrafts, electric vehicles and other applications makes integrated starter/generator (ISG) systems very interesting due to their low weight and volume [1]-[3]. The ISG has two basic functions: (1) In the starting mode, it operates as a motor and accelerates the engine to its ignition speed; (2) In the generating mode, driven by the engine, it operates as a generator and outputs electrical power. Many types of the electric machines can be used in the ISG systems, such as brushless wound-rotor synchronous machines [4]-[6], permanent-magnet synchronous machines [7]-[9], hybrid excitation synchronous machines [10], [11], switched reluctance machines [12]-[14], induction machines (IMs) [15]-[19] and so on.

IMs are a good solution for ISG systems because of their simple structure, low cost and maintenance [15]-[17]. However, the IM-based ISG systems have the limitation of the torque density and reliability in the starting mode. To overcome this drawbacks, the research on multiphase IMs-based ISG systems, for improved high torque density and fault tolerance performance, has considerably increased [18]-[20]. A shaft-line-embedded multiphase induction starter/generator for aerospace is optimized and its control strategy, for both overload capabilities and post-fault operations, is validated in [18]. A six-phase induction starter/generator is designed and

Manuscript received Oct 11, 2018; revised Nov 21, 2018, Jan 29, 2019; and Mar 14, 2019; accepted Mar 21, 2019. This work was supported in part by the National Natural Science Foundation of China (51277095, 51507079), the China Postdoctoral Science Foundation Funded Project (2014M560421, 2016T90454), and the Fundamental Research Funds for the Central Universities (NJ20160046, NS2018025).

H. Liu, F. Bu, W. Huang, L. Liu and Y. Hu are with Center for More-Electric-Aircraft Power System, the Key Laboratory of New Energy Generation and Power Conversion of Jiangsu Province, Nanjing University of Aeronautics and Astronautics, Nanjing 211106, China (e-mail: liuhaozhe1991@163.com, bufeifei1984@163.com, huangwx@nuaa.edu.cn, Liulu\_95@163.com, huyuwen@nuaa.edu.cn).

M. Degano and C. Gerada are with the Power Electronics, Machines and Control Group, University of Nottingham, Nottingham, NG7 2RD U.K., (e-mail: Michele.Degano@Nottingham.ac.uk, Chris.Gerada@Nottingham.ac.uk).

tested for mini-hybrid powertrain to obtain high starting torque and wide constant-power speed range [19], [20]. Although multiphase IMs have high torque and reliability in the starting mode, they present some problems in the generating mode. Firstly, the output voltage is difficult to regulate under the speed and load variations [21]; secondly, the high-frequency harmonics, induced by the converters' switches are transferred the loads, with negative effects on the power quality [22], [23].

To minimize the problems above, many solutions have been proposed in literature. In terms of system topology, an integrated hybrid AC/DC generating system based on an open-winding induction generator with two converters is presented in [24]. Control strategies considering model-based predictive direct torque control to get the maximum output power are considered [25]. A voltage-oriented decoupling control scheme, to reduce the voltage and current harmonics, is investigated [26]. To improve the performance, a new type of dual stator-winding induction generator (DWIG) with a static excitation controller (SEC) is proposed in [21], [22]. DWIG presents two sets of stator windings. They have no electrical connection so that the active power and reactive power of the DWIG is separated, but they are electromagnetically coupled. As the SEC mainly provides reactive power for the DWIG, its capacity is low and the high-frequency harmonics induced by switches can be minimized [21], [22], [35]. Considering these characteristics and advantages, DWIG has drawn the attention of the research community. The relevant studies are focused on topologies [21]-[23], control strategies [21]-[23], [27] optimal designs [28]-[30], modeling [31], [32] and analysis of operation states [33]-[36].

Recently, some new topologies used for DWIG system are studied [37]-[39]. To improve the voltage regulation and power quality, a new configuration of DWIG using shunt and series capacitors is presented [37]. In [38] a DC-bus-paralleled topology, with passive tuned filter and its optimal current control strategy, is studied to extend the speed range in the application of wind power. While other topologies using boost converter and DWIG are investigated [39]. Multiphase DWIG gives a number of advantages of both multiphase IMs and DWIGs. They can be employed in DC generating system with good performance and high power density, by third-harmonic injection, as shown in [40]-[42]. From the previous works, it is clear that multiphase DWIG has a great potential to be used in ISG systems. To achieve this, starter/generator control strategy is one of the most important aspects to consider. However, there is a research gap on these issues.

This paper presents an integrated starter/generator control strategy using indirect control-winding-flux-oriented control (ICWFOC) for FPDWIM-based starter/generator systems. To integrate both starting and generating controls, the operating principles and structures in different modes are kept consistent with each other by using ICWFOC. The CW current is regulated to control the CW flux and torque in the starting mode. While in the generating mode, it is regulated to control the CW and PW DC voltages. The goal is to demonstrate that during the

starting-generating operation modes, which consist of 4 steps, the physical quantities are smoothly controlled.

This paper is organized as follows. The description of the FPDWIM starter/generator system is given in Section II. Section III introduces the proposed control strategy for the whole starting-generating process. The simulation results and analysis are shown in Section IV. To validate the proposed strategy, Section V presents the experimental results and the related analysis. Some useful conclusions are drawn in Section VI.

## II. FPDWIM-BASED STARTER/GENERATOR SYSTEM

### A. System topology

The topologies of the FPDWIM-based starter/generator system, operating in different modes, are shown in Fig. 1. The FPDWIM has cage-type rotor. There are two groups of windings on its stator. The first is called five-phase CW, which is connected with the five-phase converter. The other is named five-phase PW, which is linked with the diode rectifier to output DC power. The CW and PW have the same number of pole pairs and they have no electrical connections, but they are coupled electromagnetically. In Fig. 1, a starting power and a diode  $D$  are used during the starting mode and to build-up the voltage.

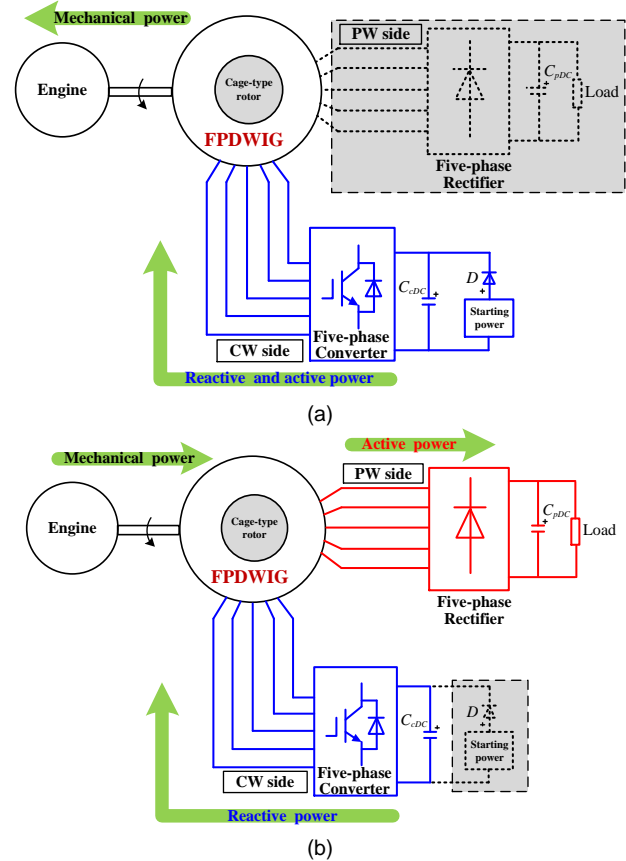


Fig. 1. The topologies of the FPDWIM-based starter/generator system. (a) Starting mode. (b) Generating mode.

As shown in Fig. 1(a) (starting mode), diode  $D$  turns on and the starting power provides both active and reactive power for

the FPDWIM through the five-phase converter. The FPDWIM operates as a motor and outputs torque to drive the engine. In this mode, the PW is not active, and the FPDWIM transfers electric power into mechanical power. Generally, the capacity of the converter in the starting mode is less than the generation capacity.

In the generating mode, the CW and the PW DC bus voltages are firstly built-up. As show in Fig. 1(b), when the CW DC bus voltage is higher than that of the starting power, diode  $D$  turns off. The five-phase converter mainly provides the reactive power for the FPDWIM. When the PW DC bus voltage reaches its target value, the system goes into the stable generating mode. The PW outputs the active power to the DC loads through a five-phase rectifier. In this mode, the FPDWIM transfers mechanical power into electric power.

This topology has three main advantages: (1) compared with three-phase IM-based S/G system, it has higher reliability because of its fault-tolerant capability; (2) compared with single-winding IM, the influence of the converter-induced high-frequency harmonics on the loads can be minimized or greatly reduced. This is mainly because the CW and PW, of the FPDWIM, have electrical separation and the loads are not connected directly with the converter; (3) the converter used in both starting and generating modes is the same one. In addition to that, its capacity is relatively small in the generating mode as the converter mainly deals with reactive power; so the hardware can be more compact to be integrated with the S/G system.

### B. Principle and analysis of the starting-generating process

The starting-generating process can be described in four steps, as shown in Fig. 2 for different variables. Fig. 3 shows the torque-speed characteristics of the system.

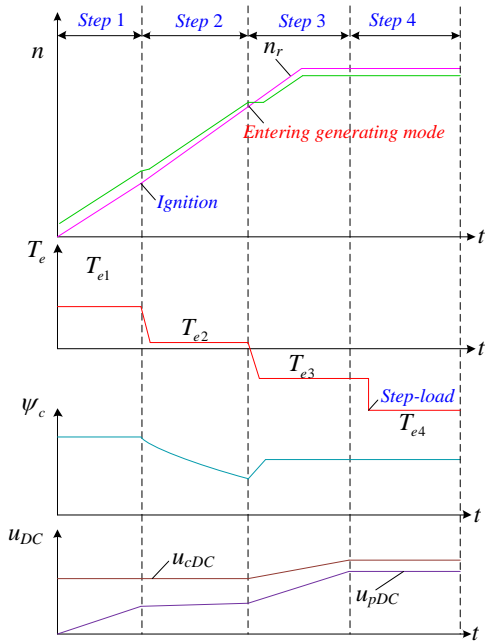


Fig. 2. The operating curves for different variables during the starting-generating process.

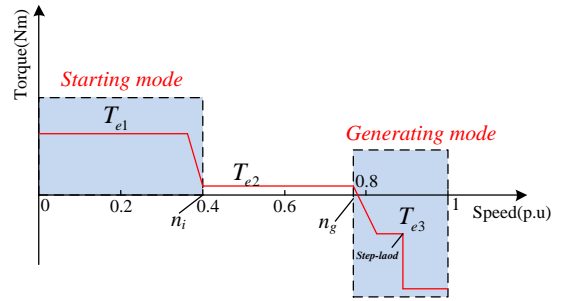


Fig. 3. The torque-speed characteristics of the FPDWIM-based S/G system.

*Step 1:* In the starting mode, the FPDWIM operates as a motor. The CW flux is constant and FPDWIM provides a positive electromagnetic torque ( $T_{e1}$ ) to drive the engine. The rotor accelerates and the stator mmf speed ( $n_c$ ) is higher than the rotor speed ( $n_r$ ).

*Step 2:* When the engine reaches the ignition speed ( $n_i$ ), it accelerates and drives the FPDWIM. The FPDWIM enters the transition process from the starting mode to the generating mode. It only needs a small positive electromagnetic torque ( $T_{e2}$ ) to overcome the no-load torque. With the rotor accelerates, the CW flux is decreased.

*Step 3:* When the rotor speed reaches the generating speed ( $n_g$ ), it is higher than the stator mmf speed. The electromagnetic torque changes from a positive to negative value ( $T_{e3}$ ). The FPDWIM enters the voltage-built-up mode and the CW flux increases gradually. Both the CW and PW DC bus voltages are increased.

*Step 4:* When the CW side and PW DC bus voltages reach to their command values respectively, the FPDWIM goes into the stable generating mode and outputs a constant negative electromagnetic torque ( $T_{e4}$ ).

To build the ISG system using the FPDWIM, a starter/generator control strategy is very important during the entire starting-generating process, which is the main contribution of this paper.

### III. PROPOSED CONTROL STRATEGY

In the generating mode, as the converter mainly provides the reactive power for the FPDWIM, the ICWFOC strategy has the advantages of easy implementation and simple flux observer. Therefore, it is suitable to control the CW and PW DC bus voltages. In terms of the ISG system, the control strategies in both starting and generating modes are expected to be compatible for the integration and good performance. In order to achieve this target, the principles and structures of the control strategies in starting and generating modes and the generating mode should be consistent. With this consideration, the ICWFOC is also used in the starting mode. An ICWFOC-based integrated starter/generator control strategy is proposed in this paper and described below.

#### A. Method of the integration of starting control and generating control

*Step 1:* In starting mode, FPDWIM operates as a motor. The CW flux should be constant to provide enough positive

electromagnetic torque ( $T_{e1}$ ) to drive the engine. The rotor accelerates and the stator mmf speed ( $n_c$ ) is higher than the rotor speed ( $n_r$ ). The voltage equations and flux equations of the FPDWIM are as follows:

$$\begin{cases} u_{cd} = R_c i_{cd} + p\psi_{cd} - \omega_c \psi_{cq} \\ u_{cq} = R_c i_{cq} + p\psi_{cq} + \omega_c \psi_{cd} \\ 0 = R_r i_{rd} - \omega_s \psi_{rq} + p\psi_{rd} \\ 0 = R_r i_{rq} + \omega_s \psi_{rd} + p\psi_{rq} \end{cases} \quad (1)$$

$$\begin{cases} \psi_{cd} = L_c i_{cd} + L_m (i_{rd} + i_{pd}) \\ \psi_{cq} = L_c i_{cq} + L_m (i_{rq} + i_{pq}) \\ \psi_{rd} = L_r i_{rd} + L_m (i_{cd} + i_{pd}) \\ \psi_{rq} = L_r i_{rq} + L_m (i_{cq} + i_{pq}) \end{cases} \quad (2)$$

In ICWFOC, the CW flux orientation is used, with the CW flux phasor fixed on the  $d$  axis. Therefore,  $\psi_{cd} = \psi_c$ ,  $\psi_{cq} = 0$ . In the starting mode, both active and reactive power are provided by the five-phase converter connected with the CW. The PW hardly outputs electric power, the PW current components ( $i_{pd}$ ,  $i_{pq}$ ) are zero ( $i_{pd} = 0$ ,  $i_{pq} = 0$ ). So (1) and (2) can be rewritten as:

$$\begin{cases} u_{cd} = R_c i_{cd} + p\psi_{cd} \\ u_{cq} = R_c i_{cq} + \omega_c \psi_{cd} \\ 0 = R_r i_{rd} - \omega_s \psi_{rq} + p\psi_{rd} \\ 0 = R_r i_{rq} + \omega_s \psi_{rd} + p\psi_{rq} \end{cases} \quad (3)$$

$$\begin{cases} \psi_{cd} = L_c i_{cd} + L_m i_{rd} \\ 0 = L_c i_{cq} + L_m i_{rq} \\ \psi_{rd} = L_r i_{rd} + L_m i_{cd} \\ \psi_{rq} = L_r i_{rq} + L_m i_{cq} \end{cases} \quad (4)$$

From the second row of the (4):

$$i_{rq} + i_{pq} = -\frac{L_c}{L_m} i_{cq} \quad (5)$$

The approximate relationship between  $i_{rq}$  and  $i_{cq}$  can be expressed as:

$$i_{rq} = -\frac{L_c}{L_m} i_{cq} \quad (6)$$

Substituting (6) into the fourth row of (4),  $\psi_{rq}$  can be expressed as follow:

$$\psi_{rq} = -\frac{L_c L_r - L_m^2}{L_m} i_{cq} \quad (7)$$

Substituting (6), (7) into the fourth rows of (1),  $\psi_{rd}$  can be rewritten as follow:

$$\psi_{rd} = \frac{1}{\omega_s} (R_r \frac{L_c}{L_m} + p \frac{L_c L_r - L_m^2}{L_m}) i_{cq} \quad (8)$$

Combining the first and third rows of (4) and (8), the CW flux  $\psi_c$  can be expressed by the CW current components:

$$\psi_c = \frac{1 + \sigma T_r p}{1 + T_r p} L_c i_{cd} - \frac{\omega_s T_r \sigma}{1 + T_r p} L_c i_{cq} \quad (9)$$

where  $\sigma$  is the magnetic leakage factor of the FPDWIM,  $\sigma = 1 - [L_m^2 / (L_c L_r)]$ ;  $T_r$  is the rotor time instant,  $T_r = L_r / R_r$ .

The electromagnetic torque  $T_e$  can be written as follow:

$$T_e = \frac{5}{2} n_p \psi_{cd} i_{cq} = \frac{5}{2} n_p \frac{1 + \sigma T_r p}{1 + T_r p} L_c i_{cd} i_{cq} \quad (10)$$

At steady state,  $p=0$ , so (9) can be rewritten as:

$$\psi_c = L_c (i_{cd} - \omega_s T_r \sigma i_{cq}) \quad (11)$$

Actually, in the FPDWIM,  $\omega_s T_r \sigma$  is negligible. Therefore, the CW flux is mainly related to  $i_{cd}$ . From (10),  $i_{cq}$  should be controlled as a constant positive value to make the FPDWIM output a starting torque. Thus, the command values of the  $i_{cd}$  and  $i_{cq}$  in *step 1* are given as follows:

$$\begin{cases} i_{cd1}^* = \frac{\psi_c^*}{L_c} \\ i_{cq1}^* = \frac{2T_{e1}}{5n_p \psi_c^*} \end{cases} \quad (12)$$

**Step 2:** When the engine ignites, it begins to accelerate and drive the FPDWIM. The FPDWIM enters the transition from starting to generating mode. In this process, it only needs a small positive electromagnetic torque ( $T_{e2}$ ) to overcome no-load torque. Therefore,  $T_e$  should be decreased from  $T_{e1}$  to  $T_{e2}$  and the CW flux should decrease gradually with the rotor speed increase. To define  $\omega_{ci}$  is the CW angular frequency at the time when the engine ignites, and the command values of  $i_{cd}$  in *step 2* are given as follow:

$$i_{cd2}^* = \frac{\omega_{ci}}{\omega_c} \frac{\psi_c^*}{L_c} = \frac{\omega_{ci}}{\omega_c} i_{cd1}^* \quad (13)$$

As the FPDWIM speed-ups together with engine, the CW angular frequency  $\omega_c$  increases. From (13),  $i_{cd}$  decreases gradually, and the CW flux also decreases gradually. To control  $T_e$  decrease from  $T_{e1}$  to  $T_{e2}$ , according to (10) and (12), the command value of the  $i_{cq}$  should be:

$$i_{cq2}^* = \frac{\omega_c}{\omega_{ci}} \frac{T_{e2}}{T_{e1}} i_{cq1}^* \quad (14)$$

From (14), when the engine ignites,  $\omega_c = \omega_{ci}$  and  $i_{cd1}^* = i_{cd2}^*$ , which means that there is no step change in the command value of  $i_{cd}$  from *Step 1* to *Step 2*. However, from (14), there will be a step change in the command value of the  $i_{cq}$ . To avoid this, a ramp from  $i_{cq1}^*$  to  $i_{cq2}^*$  is used as follow:

$$\begin{cases} i_{cq2}^* = \frac{2T_{e1}}{5n_p \psi_c^*} - kt, & i_{cq2}^* \geq \frac{2T_{e2}}{5n_p \psi_c^*} \\ i_{cq2}^* = \frac{2T_{e2}}{5n_p \psi_c^*}, & i_{cq2}^* \leq \frac{2T_{e2}}{5n_p \psi_c^*} \end{cases} \quad (15)$$

Where,  $k$  is the slope and  $t$  is time instant. In this paper, the value of  $k$  is determined as 100.

**Step 3:** When the rotor speed reaches the generating speed, the FPDWIM starts to enter the generating mode. The electromagnetic torque changes from a positive value to a negative one ( $T_{e3}$ ), and the rotor speed increases gradually beyond the stator mmf speed. From (13) and (14), the initial values of the command values of  $i_{cd}$  and  $i_{cq}$  when the FPDWIM enters in *Step 3* are as follows:

$$\begin{cases} i_{cd3-initial}^* = \frac{\omega_{ci}}{\omega_{cg}} i_{cd1}^* \\ i_{cq3-initial}^* = \frac{\omega_{cg}}{\omega_{ci}} \frac{2T_{e2}}{5n_p \psi_c^*} i_{cq1}^* \end{cases} \quad (16)$$

To achieve the voltage build-ups of both CW and PW DC bus, the CW flux increases gradually. To control the CW and PW DC bus voltage, to be their command values respectively, two voltage closed-loops with PI regulators are introduced. The command values of  $i_{cd}$  and  $i_{cq}$  are as follows:

$$\begin{cases} i_{cd3-initial}^* = \frac{\omega_{ci}}{\omega_{cg}} i_{cd1}^* + \mathbf{PI}_{pDC}(u_{pDC}^* - u_{pDC}) \\ i_{cq3-initial}^* = \frac{\omega_{cg}}{\omega_{ci}} \frac{2T_{e2}}{5n_p \psi_c^*} i_{cq1}^* - \mathbf{PI}_{cDC}(u_{cDC}^* - u_{cDC}) \end{cases} \quad (17)$$

Where,  $\mathbf{PI}_{pDC}$  is the PI regulator of the PW DC bus voltage;  $\mathbf{PI}_{cDC}$  is the PI regulator of the CW DC bus voltage.

**Step 4:** When both CW and PW DC bus voltages reach to their command values respectively, the FPDWIM enters the stable generating mode and the output a constant negative electromagnetic torque ( $T_{e4}$ ).

### B. Implementation of the proposed integrated starter/generator control strategy

Based on the analysis above, Fig. 4 shows the diagram of the proposed control strategy for the whole starting-generating process. In Fig. 4, switch  $S_1$  and  $S_2$  are used to select the command values of  $i_{cd}$  and  $i_{cq}$  in different steps, and they switch at the same time. In *Step 1*, switch  $S_1$  and  $S_2$  contacts 1; in *Step 2*, switch  $S_1$  and  $S_2$  contacts 2. In *Step 3* and 4,  $S_1$  and  $S_2$  contacts 3. The command values of  $i_{cd}$  and  $i_{cq}$  are obtained by the sum of their final values in *Step 2* and the output values of the two PI controllers. In the starting mode,  $T_e(p_c)$  and  $\psi_c(q_c)$  can be controlled by  $i_{cq}$  and  $i_{cd}$ , respectively. In the generating mode,

$u_{cDC}(p_c)$  and  $u_{pDC}(q_c)$  can be controlled by  $i_{cq}$  and  $i_{cd}$ , respectively. Either in starting or generating mode, the CW active power ( $p_c$ ) and reactive power ( $q_c$ ) are always controlled by  $i_{cq}$  and  $i_{cd}$ . Because of this control between the two modes, the control structures are consistent in different steps. Many factors should be taken into account in the parameter designs of the four PI controllers, such as the dynamic performance, the system stability. With the combination of the simulation study and practice, the parameters of four PI controllers are finally designed. The parameters of the PI controllers used in this paper are listed in Appendix.

## IV. SIMULATION RESULTS

To test the feasibility of the proposed control strategy, a simulation model is built in Matlab/Simulink environment. The parameters of the prototype are listed in Appendix. To simulate the whole starting-generating process, when the FPDWIM operates in the starting mode, the ignition speed of the engine is set as 600rpm. When the engine ignites, it accelerates itself. When the rotor speed is 1300rpm, the FPDWIM enters in the generating mode. After the starting-generating process, the FPDWIM works in the stable generating mode and a rated step-load is included. The simulation results of the whole starting-generating process are shown in Fig. 5.

It can be seen from Fig. 5 that:

(1) In *Step 1*, the FPDWIM outputs a constant positive electromagnetic torque. The CW  $q$ -axis current is maintained about 5A. Both the CW active and reactive power increase. The CW DC bus voltage is about 270V, which is determined with the consideration of the voltage rate of the common starting power and the CW phase voltage.

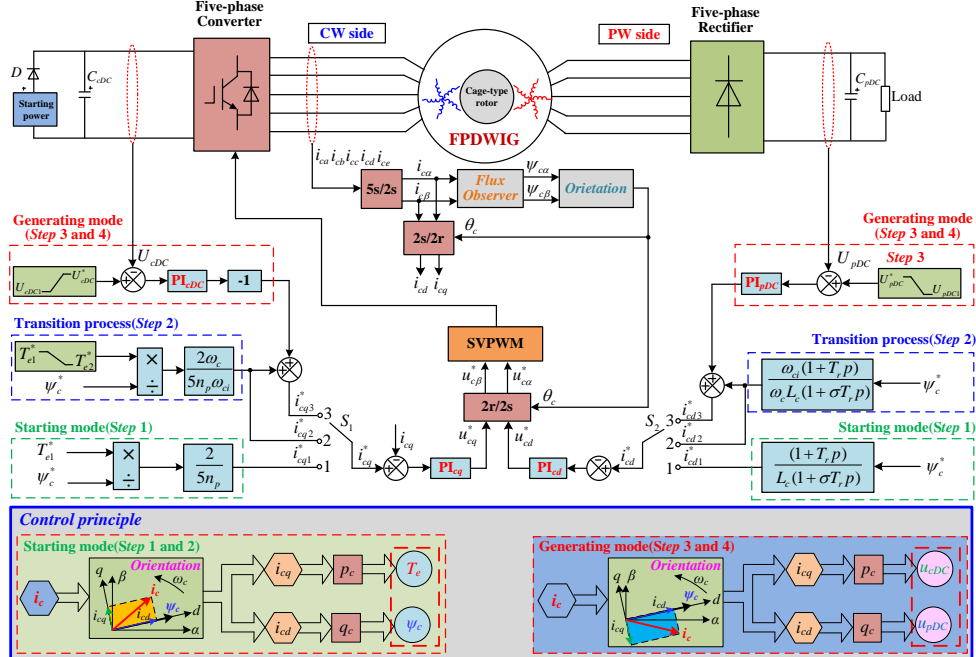


Fig. 4. The diagram of the control strategy for the whole starting-generating process.

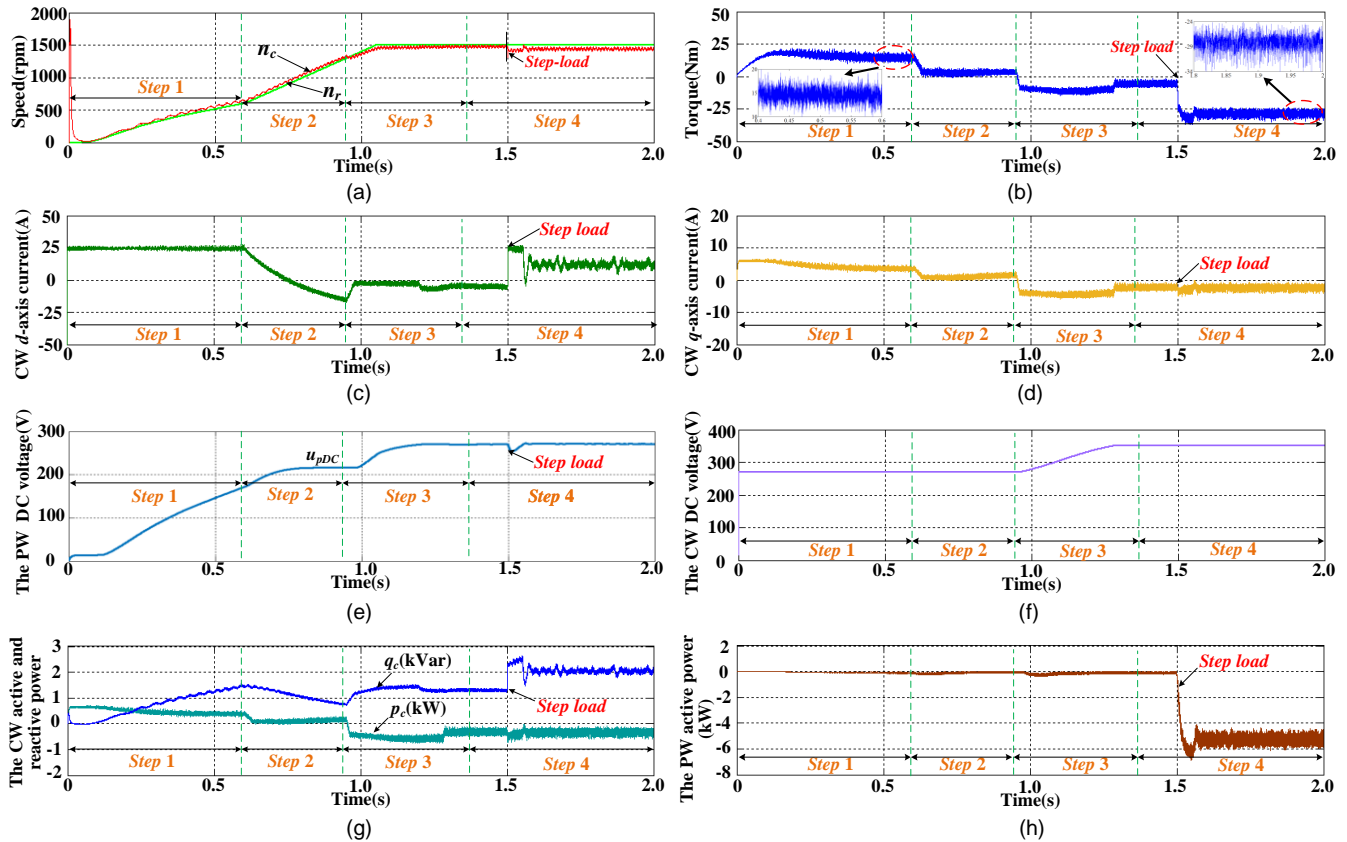


Fig. 5. The simulation results of the whole starting-generating process. (a) Rotor and stator speed. (b) Torque. (c) The CW  $d$ -axis current. (d) The CW  $q$ -axis current. (e) The PW DC bus voltage. (f) The CW DC bus voltage. (g) The CW active and reactive power. (h) The PW active power.

(2) In *Step 2*, the FPDWIM only provides a little positive electromagnetic torque to overcome the no-load torque itself. The CW  $q$ -axis current decreases from about 4A to about 1A. Correspondingly, the CW active power is very small. With the rotor speed increasing, the reactive power decrease gradually. In the starting mode, the CW does not output electric power.

(3) In *Step 3*, the electromagnetic torque of the FPDWIM decreases smoothly from positive to negative value, and the rotor speed is higher than the stator mmf speed. Both the CW and PW DC bus voltages reach to their command values (about 350V and 270V respectively). The value of the PW DC bus voltage is determined according to the voltage rate of the diode rectifier. While the value of the CW DC bus voltage is selected to guarantee that the CW DC bus can work independently in the generating mode. The CW  $q$ -axis current and active power are negative, as the CW needs output active power to maintain the CW DC bus voltage. The CW reactive power is regulated for the PW DC bus voltage build-up.

(4) In *Step 4*, the FPDWIM enters in stable generating state. The rotor speed maintains at its rated value (1500rpm). The CW and the PW DC bus voltages maintain about 350V and 270V, respectively.

(5) During the complete starting-generating process, the FPDWIM can operate steadily. All the variables have no sudden change, which means that the system can convert from the starting mode to the generating mode smoothly.

(6) With a step-load of rated power in the stable generating mode, the CW flux and  $d$ -axis current increase to make the PW DC bus voltage recover to its reference value. The CW reactive power is increased and the PW outputs about 5kW active power.

The simulation results are showing that the proposed control strategy can effectively control the whole starting-generating process and have good compatibility and performance for different steps.

## V. EXPERIMENTAL RESULTS

To verify the proposed control strategy, a prototype of the FPDWIM-based starter/generator system is built. Figs. 6 and 7 are showing the prototype of the system and the experimental setup.

A three-phase induction motor driven by Siemens 440M inverter is used to simulate the engine. The five-phase converter is composed of two Mitsubishi power modules. The proposed method is implemented in a digital signal processor (DSP) of TI TMS320F28335. An auxiliary 270V power supply is used as the starting power. Two VSM025A DC voltage sensors and four CSM100LTA current sensors are used in the test rig. In the starting mode, the three-phase induction motor provides load torque for the FPDWIM. In the generating mode, the three-phase induction motor runs as the prime mover and outputs mechanical power. The ignition speed is set as 600rpm and the generating speed is set as 1300rpm.

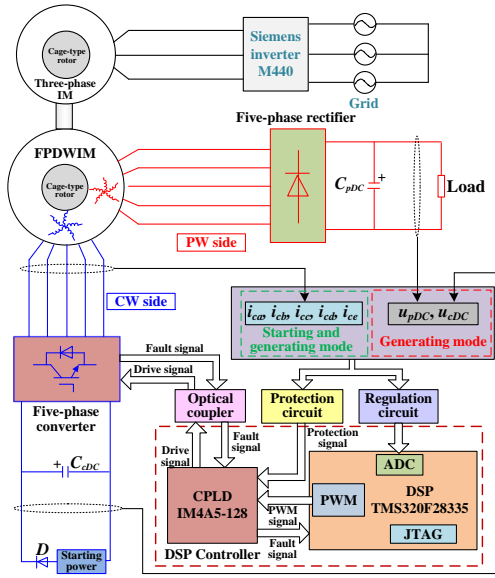


Fig. 6. The prototype of the FPDWIM-based starter/generator system.

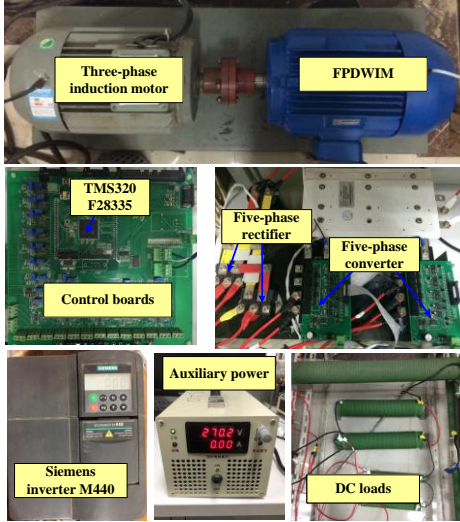


Fig. 7. Experimental setup.

### A. Experimental results of the whole starting-generating process

Fig. 8 shows the experimental results of the proposed integrated starter/generator control strategy. In Fig. 8,  $f_r$  is the rotor frequency.

From Fig. 8(a), in the starting mode, the FPDWIM operates as a motor. The CW  $d$ -axis current is controlled to a constant value of about 12A, which means that the CW flux is also unchanged. The CW  $q$ -axis current is maintained to 2.5A. The FPDWIM provides a positive starting torque. The rotor frequency increases from 0 to about 20Hz (600rpm). In this process, the starting power provides both active and reactive power for the FPDWIM. The CW side DC bus voltage is maintained to about 270V.

In Fig. 8(b), when the FPDWIM goes into the transition from starting to generating mode, the CW  $d$ -axis current is decreased, which means that the CW flux is also decreased. The CW  $q$ -axis current is controlled in a small value to provide a small positive torque to overcome the no-load torque. When the rotor

speed is over 1300rpm, the FPDWIM enters the generating mode and the CW  $d$ -axis current increases for the PW DC bus voltage ( $u_{pDC}$ ) build-up. The CW  $q$ -axis current is shifting from a positive to negative value. When  $u_{pDC}$  reaches its command value (about 270V), the FPDWIM is operating in stable generating mode.

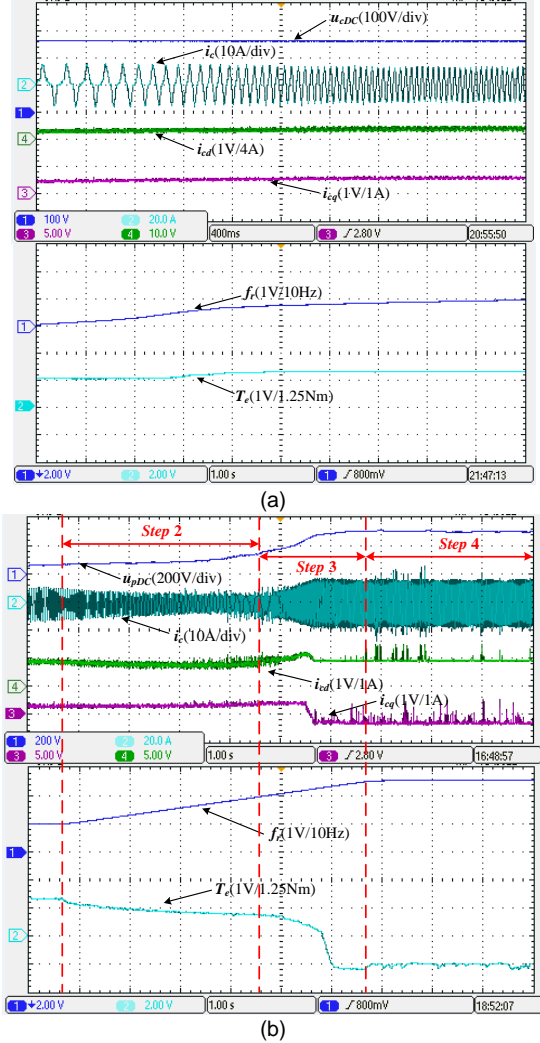


Fig. 8. Experimental results of the proposed control strategy. (a) Starting mode. (b) Transition process and generating mode.

The experimental results show that the system can perform the starting process and during the transition, between starting to generating mode, the CW  $d$ -axis and  $q$ -axis currents are continuously controlled with a good dynamic.

### B. Experimental results of the static and dynamic performance in the generating mode

To validate the static and dynamic performance of the system in the stable generating mode, further experiments are carried out and the results are shown in Fig. 9. Where,  $u_c$  is the CW voltage and  $i_{pDC}$  is the output current of the PW DC bus.

From Fig. 9(a), when the FPDWIM is generating in the steady state with rated load,  $u_{pDC}$  can maintain about 270V and the FPDWIM can stably output electric power. There is a distortion in the CW current. This is mainly caused by the

coupling between the PW and the CW. The rectifier induces the harmonic currents in the PW, which makes the CW current non-sinusoidal. The main harmonics of the CW phase current are 3<sup>rd</sup> harmonic (about 56.01%) and 7<sup>th</sup> harmonic (about 7.02%). From Fig. 9(b) and (c), the transient time with the step load and unload of 50% of the rated load are about 90ms and 100ms, respectively, and the voltage drop and rise are about 15V and 17V, respectively. In the step-load process, the PW side DC bus voltage will drop, so  $i_{cd}$  is increased firstly to provide more reactive power. After the regulation process,  $i_c$  and  $i_{cd}$  reach their new values and keep stable.

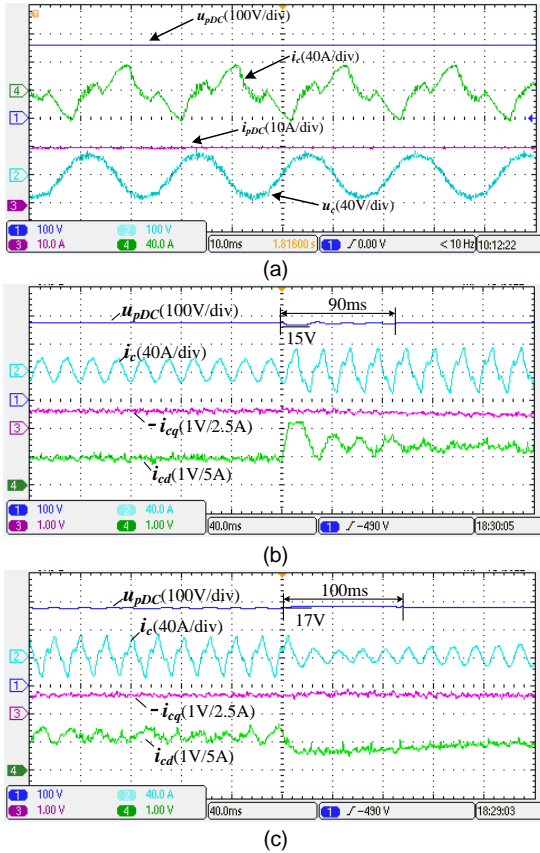


Fig. 9. Experimental results of the static and dynamic performances. (a) Static performance with rated load. (b) Step-load of 50% of rated load. (c) Step-unload of 50% of rated load.

### C. Speed range in the stable generating mode

Since the diode bridge rectifier is used, the FPDWIM can only operate above the rated speed. When this works below the base speed, it moves into deep saturation region, and the power-winding terminal voltage of the generator is too low to output the rated DC voltage by the diode bridge rectifier. The speed range of the machine in generating mode is about 1:1.5. In order to test whether the system can stably operate in constant power region, other experiments for the system working at different speeds and with rated power are carried out. Fig. 10 shows the experimental results.

From Fig. 10, at different speeds, the PW DC bus voltage maintains about 270V, and the load current is about 19.5A, which means the FPDWIM can output the rated power (5kW).

The experimental results are demonstrating that the system can work in the speed range of 1500rpm-2250rpm.

Furthermore, the proposed control strategy can accomplish the integration of the different control strategies in different modes. The system can achieve a stable operation during the starting-generating process as well as a smooth transition. The results presented are showing good static and dynamic performance, in generating mode.

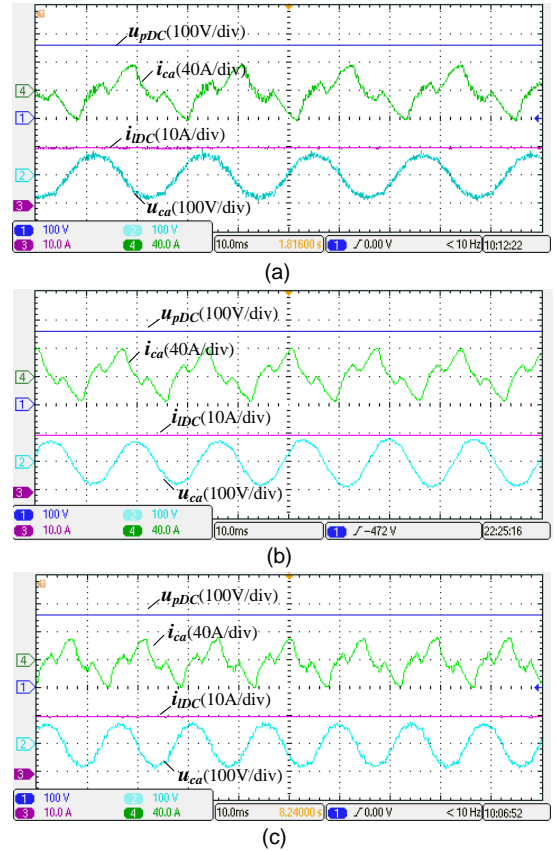


Fig. 10. The experimental results in the generating mode with rated power at different speeds. (a) At 1500rpm. (b) At 1875rpm. (c) At 2250rpm.

## VI. CONCLUSION

A control strategy for FPDWIM-based S/G system is proposed in this paper. To achieve the integration of the starting control and generating control, ICWFOC is employed in both starting and generating modes. In the starting mode, both active power and reactive power are provided by the CW through five-phase converter. The CW  $d$ -axis and  $q$ -axis currents are controlled unchanged to obtain the constant flux and enough starting torque. While in the generating mode, the CW mainly provides reactive power and the PW outputs DC electric power through the rectifier. Two voltage-loops are introduced to regulate both CW and PW DC bus voltages, and the CW  $d$ -axis and  $q$ -axis currents are regulated according to the CW and PW DC bus voltages. With the consistent structures and principles in the control strategies, and for different modes, the integrated starter/generator control is achieved. The implementation is simple and shows good performance. The simulation and experimental results are confirming the validity of the proposed control strategy. The system can steadily work over the whole

starting-generating process, and both dynamic and static performance in the generating mode have been achieved with satisfactory results.

As an S/G system, there are still many aspects that require further research, such as the improvement of the power density, sensorless-control, fault-tolerant control and so on.

#### APPENDIX

The main parameters of the prototype are as follow:

$R_c=0.19\Omega$ ;  $R_p=0.45\Omega$ ;  $R_r=0.29\Omega$ ;  
 $L_c=10.25\text{mH}$ ;  $L_r=10.29\text{mH}$ ;  $L_p=10.24\text{mH}$ ;  $L_m=10.05\text{mH}$ ;  
 Pole pairs:2; Rated power: 5kW;  
 Rated speed of the prime mover: 1500rpm;  
 Turn ratio of the power winding to the control winding: 2:1;  
 The CW side DC bus capacitor: 4400 $\mu\text{F}/450\text{V}$ ;  
 The PW side DC bus capacitor: 4400 $\mu\text{F}/450\text{V}$ ;  
 The PW side output DC bus voltage: 270V;  
 Voltage of starting power: 270V.  
 Rated phase voltage of the PW: 100V;  
 Rated phase current of the PW: 11A;  
 Rated phase voltage of the CW: 53V;  
 Rated phase current of the CW: 20A.  
 Open-circuit (no-load) characteristics:  
 Open-circuit phase current of the CW: 5A;  
 Open-circuit phase EMF voltage of the CW: 51V;  
 Open-circuit phase current of the PW: 0A;  
 Open-circuit phase EMF voltage of the PW: 102V;  
 The parameters of the four PI controllers:  
 $i_{cd}$  PI controller:  $K_{p1}=5$ ;  $K_{i1}=90$ ;  
 $i_{cq}$  PI controller:  $K_{p2}=5$ ;  $K_{i2}=10$ ;  
 $u_{pDC}$  PI controller:  $K_{p3}=2$ ;  $K_{i3}=10$ ;  
 $u_{cDC}$  PI controller:  $K_{p4}=5$ ;  $K_{i4}=10$ .

#### REFERENCES

- [1] G. Friedrich and A. Girardin, "Integrated starter generator," *IEEE Ind. Appl. Mag.*, vol. 15, no. 4, pp. 26–34, Jul./Aug. 2009.
- [2] S. Bhangu and K. Rajashekhara, "Electric starter generators: Their integration into gas turbine engines," *IEEE Ind. Appl. Mag.*, vol. 20, no. 2, pp.14–22, Mar./Apr. 2014.
- [3] B. Sarioglu and C. T. Morris, "More electric aircraft: Review, challenges, and opportunities for commercial transport aircraft," *IEEE Trans. Transp. Electrification*, vol. 1, no. 1, pp. 54–64, Jun. 2015.
- [4] Z. Zhang, W. Liu, D. Zhao, S. Mao, T. Meng, and Ningfei Jiao "Steady-state performance evaluations of three-phase brushless asynchronous excitation system for aircraft starter/generator," *IET Electr. Power Appl.*, vol. 10, no. 8, pp. 788–798, 2016.
- [5] A. Griffio, R. Wrobel, P. H. Mellor, and J. M. Yon, "Design and characterization of a three-phase brushless exciter for aircraft starter/generator," *IEEE Trans. Ind. Appl.*, vol. 49, no. 5, pp. 2106–2115, Sep./Oct. 2013.
- [6] A. Griffio, D. Drury, T. Sawata, and P. H. Mellor, "Sensorless starting of a wound-field synchronous starter/generator for aerospace applications," *IEEE Trans. Ind. Electron.*, vol. 59, no. 9, pp. 3579–3587, Sep. 2012.
- [7] S. Bozhko, M. Rashed, C. I. Hill, S. S. Yeoh, and T. Yang, "Flux weakening control of electric starter-generator based on permanent magnet machine," *IEEE Trans. Transp. Electrification*, vol. 3, no. 4, pp. 864–877, Dec. 2017.
- [8] J.-H. Seo, S.-M. Kim, and H.-K. Jung, "Rotor-design strategy of ipmsm for 42v integrated starter generator," *IEEE Trans. Magn.*, vol. 46, no. 6, pp. 2458–2461, Jun. 2010.
- [9] Z. Zhang, J. Huang, Y. Jiang, W. Geng and Y. Xu "Overview and analysis of pm starter/generator for aircraft electrical power systems," *CES Trans. Electrical machines and systems*, vol. 1, no. 2, pp. 117–131, Jun. 2017.
- [10] Z. Zhang, J. Li, Y. Liu, Y. Xu, and Y. Yan, "Overview and development of variable frequency ac generators for more electric aircraft generation system," *Chinese Journal of Electrical engineering*, vol. 3, no. 2, pp.32–40, Sep. 2017.
- [11] C. Han, B. Zhou, and J. Wei, "Modeling and simulation of hybrid excitation synchronous starter/generator system," in *Proc. Int. Conf. Elect. Control Eng.*, Jun. 2010, pp. 5533–5536.
- [12] W. Ding and D. Liang, "A fast analytical model for an integrated switched reluctance starter/generator," *IEEE Trans. Energy Convers.*, vol. 25, no. 4, pp. 948–956, Dec. 2010.
- [13] N. Schofield and S. Long, "Generator operation of a switched reluctance starter/generator at extended speeds," *IEEE Trans. Veh. Technol.*, vol. 58, no. 1, pp. 48–56, Jan. 2009.
- [14] C. Ferreira, S. R. Jones, W. S. Heglund, and W. D. Jones, "Detailed design of a 30kW switched reluctance starter/generator system for a gas turbine engine application," *IEEE Trans. Ind. Appl.*, vol. 31, no. 3, pp. 553–561, May/Jun. 1995.
- [15] M. E. Elbuluk and M. D. Kankan, "Potential starter/generator technologies for future aerospace applications," *IEEE Aerosp. Electron. Syst. Mag.*, vol. 12, no. 5, pp. 24–31, May, 1997.
- [16] I. Alan and T. A. Lipo, "Starter/generator employing resonant-converter-fed induction machine part I: Analysis," *IEEE Trans. Aerosp. Electron. Syst.*, vol. 36, no. 4, pp. 1309–1318, Oct. 2000.
- [17] I. Alan and T. A. Lipo, "Starter/generator employing resonant-converter-fed induction machine part II: Hardware prototype," *IEEE Trans. Aerosp. Electron. Syst.*, vol. 36, no. 4, pp. 1319–1329, Oct. 2000.
- [18] R. Bojoi, A. Cavagnino, A. Tenconi, and S. Vaschetto, "Control of shaft-line-embedded multiphase starter/generator for aero-engine," *IEEE Trans. Ind. Electron.*, vol. 63, no. 1, pp. 641–652, Jan. 2016.
- [19] R. Bojoi, A. Cavagnino, M. Cossale, and A. Tenconi, "Multiphase starter generator for a 48-v mini-hybrid powertrain: design and testing," *IEEE Trans. Ind. Appl.*, vol. 52, no. 2, pp. 1750–1758, Mar./Apr. 2016.
- [20] A. Cavagnino, A. Tenconi, and S. Vaschetto, "Experimental characterization of a belt-driven multiphase induction machine for 48-v automotive applications: losses and temperatures assessments," *IEEE Trans. Ind. Appl.*, vol. 52, no. 2, pp. 1321–1330, Mar./Apr. 2016.
- [21] O. Ojo and I. E. Davidson, "Pwm-vsi inverter-assisted stand-alone dual stator winding induction generator," *IEEE Trans. Ind. Appl.*, vol. 36, no. 6, pp. 1604–1611, Nov./Dec. 2000.
- [22] D. Wang *et al.*, "A novel stand-alone dual stator-winding induction generator with static excitation regulation," *IEEE Trans. Energy Convers.*, vol. 20, no. 4, pp. 826–835, Dec. 2005.
- [23] F. Bu, Y. Hu, W. Huang, S. Zhuang, and K. Shi, "Wide-speed-range-operation dual stator-winding induction generator dc generating system for wind power applications," *IEEE Trans. Power Electron.*, vol. 30, no. 2, pp. 561–573, Feb. 2015.
- [24] Y. Jia and K. Rajashekhara, "An induction generator-based ac/dc hybrid electric power generation system for more electric aircraft," *IEEE Trans. Ind. Appl.*, vol. 53, no. 3, pp. 2485–2494, May/Jun. 2017.
- [25] A. S. Lunardi, J. S. S. Chaves, and A. J. S. Filho, "Predictive direct torque control for a squirrel cage induction generator grid connected for wind energy applications," *IEEE Latin America Transaction*, vol. 14, no. 11, pp. 4454–4461, Nov. 2016.
- [26] S. M. Mahajan, S. Se. Kumar, N. Kumaresan, N. G. A. Gounden, and E. Rajkumar "Decoupled control strategy for the operation of capacitor-excited induction generator for dc power applications," *IET Power Electron.*, vol. 9, no. 13, pp. 2551–2561, 2016.
- [27] S. Basak and C. Chakraborty, "Dual stator winding induction machine: problems, progress, and future scope," *IEEE Trans. Ind. Electron.*, vol. 62, no. 7, pp. 4641–4652, Jul. 2015.
- [28] H. Xu, F. Bu, W. Huang, Y. Hu, H. Liu and Y. Zhao, "Analysis, comparison, and discussion of control strategies for dual stator-winding induction generator dc generating system," *IEEE JEST. Power Electron.*, vol. 4, no. 3, pp. 1007–1014, Sep. 2016.
- [29] Y. Li, Y. Hu, W. Huang, L. Liu, and Y. Zhang, "The capacity optimization for the static excitation controller of the dual-stator-winding induction generator operating in a wide speed range," *IEEE Trans. Ind. Electron.*, vol. 56, no. 2, pp. 530–541, Feb. 2009.

- [30] F. Bu, W. Huang, Y. Hu, and K. Shi, "An excitation-capacitor-optimized dual stator-winding induction generator with the static excitation controller for wind power application," *IEEE Trans. Energy Convers.*, vol. 26, no. 1, pp. 122–131, Mar. 2009.
- [31] L. N. Tutelea, S. I. Deaconu, I. Boldea, and N. Budisan, "Design, control and 2D-FEM validation for a double stator winding induction generator," in *Proc. IEEE IECON*, pp. 2732–2737, Nov. 2003.
- [32] Y. Yao and L. Li, "Study on double winding stator induction generator system," in *Proc. IEEE ICECC*, pp. 2313–2315, Sep. 2011.
- [33] J. A. Barrado-Rodrigo, J. I. Talpone, and L. Martínez-Salamero, "Variable-speed wind energy conversion system based on a dual stator winding induction generator," *IET Renewable Power Generation*, vol. 11, No. 1, pp. 73–80, 2017.
- [34] M. Moradian and J. Soltani, "An isolated three-phase induction generator system with dual stator winding sets under unbalanced load condition," *IEEE Trans. Energy Convers.*, vol. 31, no. 2, pp. 531–539, Jun. 2016.
- [35] M. H. Zamani, G. H. Riahy and M. Abedi, "Rotor-speed stability improvement of dual stator-winding induction generator-based wind farms by control-winding voltage oriented control," *IEEE Trans. Power Electron.*, vol. 31, no. 8, pp. 5538–5546, Aug. 2016.
- [36] F. Bu, S. Zhuang, W. Huang, N. Su and Y. Hu, "Asymmetrical operation analysis for dual stator-winding induction generator variable frequency AC generating system with unbalanced loads," *IEEE Trans. Ind. Electron.*, vol. 64, no. 1, pp. 52–59, Jan. 2017.
- [37] S. Basak and C. Chakraborty, and B. C. Pal, "A new configuration of dual stator induction generator employing series and shunt capacitors," *IEEE Trans. Energy Convers.*, vol. 33, no. 2, pp. 762–772, Jun. 2018.
- [38] S. Basak and C. Chakraborty, "A new optimal current control technique for dual stator winding induction generator," *IEEE JEST. Power Electron.*, vol. 5, no. 2, pp. 820–832, Jun. 2017.
- [39] A. Kavousi, S. H. Fathi, J. Milimonfared, and M. N. Soltani, "Application of boost converter to increase the speed range of dual-stator winding induction generator in wind power system," *IEEE Trans. Power Electron.*, vol. 33, no. 11, pp. 9599–9610, Nov. 2018.
- [40] H. Liu, F. Bu, W. Huang, and H. Xu, "Modeling of five-phase dual stator-winding induction generator with 3rd harmonic injection," in *Proc. IEEE PDES*, Sydney, Australia, Jun. 9–12, 2015, pp. 231–234.
- [41] H. Xu; F. Bu; W. Huang; Y. Hu; H. Liu, "Control and performance of five-phase dual stator-winding induction generator dc generating system," *IEEE Trans. Ind. Electron.*, vol. 64, no. 7, pp. 5276–5285, Jul. 2017.
- [42] L. Zheng, J. E. Fletcher, B. W. Williams, and X. He, "Dual-plane vector control of a five-phase induction machine for an improved flux pattern," *IEEE Trans. Ind. Electronics.*, vol. 55, no. 5, pp. 1996–2004, May. 2008.



**Haozhe Liu** was born in Zhengzhou, China in 1991. He received the B.S. degree in Electrical Engineering from Shanghai Institute of Technology, Shanghai, China, in 2014 and Master's degree from Nanjing University of Aeronautics and Astronautics (NUAA), Nanjing, China in 2017. He is currently pursuing the Ph. D degree in NUAA, Nanjing, China. His research interests are power electronics and electrical machines.



**Feifei Bu** (M'11) was born in Maanshan, China, in 1984. He received the B.S. degree in electrical engineering from Anhui University of Technology, Maanshan, China, in 2006, and the Ph.D. degree (master–doctorate program) in electrical engineering from Nanjing University of Aeronautics and Astronautics (NUAA), Nanjing, China, in 2014. He joined the faculty of the Department of Electrical Engineering, NUAA, where he is currently an Associate Professor. His research interests include power electronics and electrical machines for standalone power systems, renewable energy generating systems, electric vehicle driving systems, etc.



**Wenxin Huang** (M'09) was born in Dongtai, China, in 1966. He received the B.S. degree in the Southeast University, Nanjing, China, in 1988, and the Master's and Ph.D. degrees from Nanjing University of Aeronautics and Astronautics (NUAA), Nanjing, China, in 1994 and 2002, respectively. In 2003, he joined the faculty of the College of Automation Engineering, NUAA, where he is currently a Professor. His research interests include stand-alone power systems, power electronics, electrical machine systems.



**Lu Liu** received the B. S. degree in electrical engineering from Northwestern Polytechnical University, Xi'an, China, in 2017. He is working towards his master degree in Nanjing University of Aeronautics and Astronautics. His research interest focuses on the starter/generator system for aircraft electrical power systems.



**Yuwen Hu** (M'09) was born in Zhangshu, Jiangxi Province, China, in 1944. He received the B.S. degree in 1966 from Jiangxi University (now Nanchang University), Nanchang, China, and the Master's degree from the Nanjing Aeronautical Institute (now Nanjing University of Aeronautics and Astronautics, NUAA), Nanjing, China, in 1981. He worked at the Jiangxi Machine Tools Factory from 1967 to 1977. He later joined the NUAA. From 1986 to 1987, he worked as a visiting scholar at Kyushu University, Fukuoka, Japan. From 1995 to 1996 and from 2001 to 2002 he has been the visiting scholar in the University of New South Wales, Sydney, Australia. Now He is the Professor in NUAA. His research interests are in the power electronics, electrical machines, and motion control system.



**Michele Degano** (M'15) received the Laurea degree in electrical engineering from the University of Trieste, Trieste, Italy, in 2011, and the Ph.D. degree in industrial engineering from the University of Padova, Padova, Italy, in 2015. In 2015, he joined the Power Electronics, Machines and Control Group, The University of Nottingham, Nottingham, U.K., as a Research Fellow, where he is currently an Assistant Professor teaching advanced courses on electrical machines. His main research interests include design and optimization of permanent-magnet machines, reluctance and permanent-magnet-assisted synchronous reluctance motors through genetic optimization techniques, for automotive and aerospace applications.



**Chris Gerada** (M'05) received the Ph.D. degree in numerical modeling of electrical machines from The University of Nottingham, Nottingham, U.K., in 2005. He subsequently worked as a Researcher with The University of Nottingham on high-performance electrical drives and on the design and modeling of electromagnetic actuators for aerospace applications. Since 2006, he has been the Project Manager of the GE Aviation Strategic Partnership. In 2008, he was appointed as a Lecturer in electrical machines; in 2011, as an Associate Professor; and in 2013, as a Professor at The University of Nottingham. His main research interests include the design and modeling of high-performance electric drives and machines. Prof. Gerada serves as an Associate Editor for the IEEE Transactions on Industry Applications and is the past Chair of the IEEE IES Electrical Machines Committee.